Single-ion conducting "polymer-in-ceramic" hybrid electrolyte with intertwined NASICON-type nanofiber skeleton

Shicheng Yu[a,], Qi Xu[a,b], Xin Lu[a,b], Zigeng Liu[a], Anna Windmüller[a], Chih-Long Tsai[a], Annika Buchheit[c], Hermann Tempel[a], Hans Kungl[a], Hans-Dieter Wiemhöfer[c] and Rüdiger-A. Eichel[a,b,c]*

[a]*Institut für Energie- und Klimaforschung (IEK-9: Grundlagen der Elektrochemie), Forschungszentrum Jülich, D-52425 Jülich, Germany*

[b]*Institut für Materialien und Prozesse für elektrochemische Energiespeicher- und wandler, RWTH Aachen University, D-52074 Aachen, Germany*

[c]*Institut für Energie- und Klimaforschung (IEK-12: Helmholtz-Institute Münster, Ionics in Energy Storage), Forschungszentrum Jülich, D-48149 Münster, Germany*

KEYWORDS: polymer in ceramic, hybrid electrolyte, LATP fibers, single-ion conducting polymer, LiSTFSI

ABSTRACT: The ionic conductivity of "polymer-in-ceramic" electrolytes is highly dependent on the long-range Li^+ migration pathways, which are determined by the structure and chemistry of the electrolytes. Besides, Li dendrite growth may be promoted in the soft polymer region due to the inhomogeneous electric field caused by the commonly low Li^+ transference number of polymer. Herein, single-ion conducting polymer electrolyte is infiltrated into intertwined $Li_{1.3}Al_{0.3}Ti_{1.7}(PO_4)_3$ (LATP) nanofibers to fabricate free-standing electrolyte membranes. The composite electrolyte possesses a high potential window exceeding 5 V (vs. Li/Li^+), a high ionic conductivity of 0.31 mS cm^{-1} at ambient temperature and a high Li^+ transference number of 0.94. The hybrid electrolyte in Li symmetric cell shows stable Li plating/stripping cycling up to 2000 h under 0.1 mA cm^{-2} without dendrite formation.

The Li|hybrid electrolyte|$LiFePO_4$ battery exhibits enhanced rate capability up to 1C and stable cycling performance with an initial discharge capacity of 131.8 mAh g^{-1} and a retention capacity of 122.7 mAh g^{-1} after 500 cycles at 0.5C at ambient temperature. The improved electrochemical performance is attributed to the synergistic effects of the LATP nanofibers and the single-on conducting polymer. The fibrous fast ion conductors provide continuous ion transport channels, and the polymer improves the interfacial contact with the electrodes and helped to suppress the Li dendrites.

1. INTRODUCTION

Solid-state Li batteries promise a way to address the safety issue and realize high energy density,[1] by replacing flammable liquid electrolytes with solid electrolytes and using metallic lithium anode (high specific capacity ≈3860 mAh g^{-1}).[2,3] However, high interfacial resistance caused by the insufficient solid/solid contact, low ionic conductivity of solid electrolyte at ambient temperature and Li dendrite growth through electrolyte are the bottlenecks that hinder the realization of those promises and scale application of solid-state Li metal batteries.[4–6] To overcome the above issues, the development of high-performance solid electrolytes is essential for the practical application of solid-state Li-metal batteries.

Solid electrolytes can be divided into polymer electrolytes, ceramic electrolytes and hybrid electrolytes. Polymer electrolytes contain soft polymer matrix and Li salts, which possess high flexibility, excellent scalability, and good interfacial contact with electrodes, while mostly suffering from serious disadvantages of low ionic conductivity at room temperature ($<10^{-4}$ S cm^{-1}), inferior thermal stability, and unsatisfactory behavior in suppression of Li dendrite growth due to low Li^+ transference number (<0.5).[7–9] On the contrary, the ceramic electrolytes show high room temperature ionic conductivity (10^{-3}-10^{-2} S cm^{-1}) and mechanical strength, but difficult manufacturability and interfacial contact with electrodes.[10–13] The hybrid electrolytes constructed by organic and Li^+ conductive inorganic fillers aim to inherit the major advantages

of both polymer and ceramic electrolytes such as high ionic conductivity, good flexibility and intimate contact with electrodes. Therefore, hybrid electrolytes are considered as one of the most promising electrolytes for solid-state Li metal batteries.[14,15]

The ionic conductivity of hybrid electrolytes is mainly determined by the synergistic effects of different ion transfer mechanisms. In the bulk of conductive ceramic, Li^+ transfer depends mainly on the movement of vacancies or interstitial ions, resulting in rapid ion movement,[16,17] while the Li^+ transport in the polymer region is related to the breaks/formations of coordination bonds during the local segmental motions of polymer chains, which mainly occurs in the amorphous sections.[18–20] In addition to the conductive channels in polymer and ceramic phases, the ceramic fillers can enhance Li salt dissociation, interface conductivity, and anion attraction, or act as a Li^+ source that can also improve the overall ionic conductivity.[21,22] On the one hand, the ceramic electrolyte fillers increase the free volume in the random polymer structure near the ceramic region by facilitating the local polymer and ion mobility, and promoting any structural adaptation of the polymer chains towards ion transport or interfaces. Hence, the segmental motion of the polymer is enhanced and with it the mobility of cations and anions.[23,24] Another important factor regarding the preferential interaction (or adsorption) of the polymer/ceramic interface is the electrochemical equilibrium of lithium ions because they are mobile in both phases. Therefore, the equilibration of Li^+ will lead to the transfer of a small entity of cations. The direction of this transfer depends on the relative electrochemical potential of Li^+ ions of the two contacting phases. If the value is higher in the ceramic, there will be a small net transfer of positive charge due to excess Li^+ in the polymer near the interface. If the electrochemical potential of Li^+ is higher in the polymer electrolyte, then the contrary will be true. In both cases, there may be a negative or positive surface space charge region which acts as an expressway for ion transport in hybrid electrolyte.

Furthermore, according to Lewis acid–base theory, the acidic groups on the surface of ceramics have strong affinity with anions, which enhances the dissociation of Li salts, resulting in increased concentration of free Li^+ and higher ion mobility in the polymer near the internal interfaces to the ceramic electrolyte.[25–28] Besides, numerous vacancies and interstitial surface sites generally exist along the surfaces regions of ceramic grains which allow Li^+ hopping thus providing a faster pathway along with the ceramic/polymer interface than in the bulk polymer phase.[26,29–31]

Although the interface between polymer and ceramic filler undoubtedly creates a region with differing defect concentrations and therefore modified Li^+ mobility and sometimes leads to a fast transport channel for Li^+,[25,29–32] due to the complex Li^+ transportation, the reported ionic conductivities of hybrid electrolytes show significant variation even for the same combination of materials.[32–36] This is mainly due to the tuning-synergy effects on Li^+ transport paths in polymer, bulk ceramic, and polymer/ceramic interface region (interphase) in hybrid electrolytes, since the Li^+ transport pathways can be greatly influenced by the composition and structure of dispersed solid-state electrolyte particles. Zheng and coworkers[36] investigated this tuning-synergy effect in garnet LLZO-PEO/LiTFSI composite. With a low proportion of LLZO, the Li ions preferentially transport through the polymer phase or the polymer/ceramic interface. With increasing filler content, the main migration pathways shifts to the LLZO phase as a continuous ceramic phase with higher conductivity is formed. Similar observations were reported by other groups with different material combinations.[29,34,35] Hence, rational tuning the structural ratio between polymer and ceramic to guarantee a sufficient amount of interphase and highly conductive long-range Li^+ transport pathways could improve the ionic conductivity of the hybrid electrolyte.

Similar to polymer electrolytes, hybrid electrolytes undergo Li dendrite growth owing to the generally low Li^+ transference number of polymer.[37–39] To date, two methods have been

proposed to suppress Li dendrite growth for solid electrolytes. Chazalviel et al.[38,40,41] suggested that anion depletion near the Li electrode could lead to large electric fields, which causes preferred dendrite growth due to strongly limited local Li^+ transport so that high concentration gradients (and high overpotentials at the anode) are implied. Hence, electrolytes with low anion mobility (i.e., ceramic electrolytes, high Li^+ transference number polymers) and high Li^+ mobility can reduce the local electric field to suppress Li dendrite growth.[42–45] Another approach proposed by Monroe and Newman is to mechanically block the growth of Li dendrites.[46] If the shear modulus of the electrolyte is high enough, ideally about twice that of metallic lithium, the dendrites can be suppressed.[46] Thus, hybrid electrolytes with a high Li^+ transference number and high shear modulus could effectively suppress Li dendrite growth in solid-state Li batteries.[28,47]

In this work, one of the most ion conductive NASICON compounds, $Li_{1.3}Al_{0.3}Ti_{1.7}(PO_4)_3$ (LATP), was prepared by electrospinning and combined with a conductive polymer of cross-linked poly[bis(2-(2-methoxyethoxy) ethoxy) phosphazene] (MEEP) and lithium 4-styrenesulfonyl (trifluoromethanesulfonyl) imide (LiSTFSI) to fabricate a single-ion conducting "polymer-in-ceramic" electrolyte. We applied the chemical concept from Meziane et al. for the immobilization of anions by integrating a cross-linkable alkene group within the anion.[44] But instead of PEO as the solvent matrix, MEEP was chosen due to it much lower glass transition as compared to the PEO. Nevertheless, two short PEO chains per phosphorous along the MEEP backbone build up a polymeric solvent structure closely related to PEO with higher ionic conductivity at ambient temperatures. As compared to our previous work with MEEP/LiTFSI,[15] the use of the salt LiSTFSI instead of LiTFSI with the step to a high lithium ion transference number delivered the decisive improvement for the hybrid electrolyte as used in this work. The large fraction of 3D intertwined LATP skeleton provides the necessary structural reinforcement of the hybrid electrolyte and ensures long-range fast Li^+ migration

through the nanofibers and the high volume of interphase, leading to an enhanced ionic conductivity. Utilization of single-ion conducting polymer realized good compatibility and stability of the hybrid electrolyte against Li anode due to the high Li^+ transference number (0.94) and good wetting ability of the polymer. Through the synergistic enhancement of LATP nanofibers and polymer modification, the Li|hybrid electrolyte|$LiFePO_4$ cells show good rate performance and cycle stability at room temperature.

2. RESULTS AND DISCUSSION

2.1. Preparation of Hybrid Electrolyte.

The hybrid electrolytes were fabricated by a simplistic and efficient approach sketched in **Figure 1**. 3D intertwined NASICON-type LATP nanofibers were prepared by electrospinning of PEO solution mixed with relevant Li-Al-Ti-P-O salts followed by the calcination of the as-prepared nanofibers at 900 °C in air for 4 hours. On the drum collector of the electrospinning setup, a thin aluminum foil was covered to collect the nanofibers. Separately, the Li salt monomer (LiSTFSI) and poly[bis(2-(2-methoxyethoxy) ethoxy) phosphazene] polymer (MEEP) were respectively synthesized. The detailed material preparation can be found in the experimental section in supplementary information. The LiSTFSI being the product of synthesis was confirmed by nuclear magnetic resonance spectroscopy (^{1}H NMR, ^{13}C NMR, ^{19}F NMR) and attenuated total reflection infrared spectroscopy (ATR-IR), as shown in Figure S1-S4. The MEEP was characterized by ATR-IR (Figure S4).

The homogenous precursor solution of LiSTFSI, MEEP, benzophenone and calcined LATP nanofibers was placed between two Mylar foils and pressed to the desired thickness. After exposure to UV light, polymerization was initiated and a free-standing hybrid electrolyte membrane, consisting of the single-ion conducting polymer and the 3D intertwined LATP nanofiber skeleton backbone, was obtained. As illustrated in **Figure 1**, the volume ratio of

LATP in the hybrid structure is high, which guarantees a sufficient amount of interface regions between ceramic and polymer. The interface regions are considered to be more Li^+ conductive than the bulk polymer due to the filler effects and therefore improve the overall electrochemical performance of the hybrid electrolyte.[26,29,32]

2.2. Structure and Electrochemical Properties of LATP Nanofibers.

Morphologies of the as-spun and calcined LATP nanofibers were measured by SEM as presented in **Figure 2**a. Before calcination, the as-spun LATP-PEO salt fibers have smooth surfaces and an average diameter of 744 nm. After the calcination at 900 °C in air, PEO polymer and other intermediate products were combusted, and LATP fabric was prepared. The average diameter of the nanofibers is decreased to 389 nm. Moreover, due to high temperature treatment, LATP nanofibers were "interwelded" with each other, forming cross-linked 3D LATP nanofiber networks. The still large volume of the interspace between nanofibers can facilitate Li salt-polymer infiltration to form the hybrid electrolyte.

Thermogravimetric analysis (TGA) was applied to investigate the LATP fabric formation during the calcination process. The TGA was carried out under mixed nitrogen and oxygen (78:22) flow with a heating rate of 2 °C/min. **Figure 2**b demonstrations the TGA profile of the as-spun fibers containing PEO and LATP precursor. The mass loss in the temperature range up to 120 °C is indicating the loss of water. The significant weight loss between 120 and 500 °C is mainly due to the loss of ammonia from the LATP precursor and the complete decomposition of the polymer. When the temperature was further increased to 900 °C, a loss of only 3 wt.% was observed, which can be attributed to the complete removal of the carbon residues. The result also indicates that, above 650 °C, the weight became stable, signifying that thermally stable Li-Al-Ti-P-O nanofibers were formed. The high thermal stability of LATP ceramic skeleton in the hybrid electrolyte brings in advantages regarding safety concerns, because the

LATP nanofiber membrane forms a ceramic barrier that physically blocks contact between the cathode and anode even after the polymer is lost at high temperatures.[48,49]

Powder X-ray diffraction (XRD) measurement of calcined LATP nanofibers was carried out. As shown in **Figure 2**c, the main reflexes are assigned to rhombohedral symmetry space group R-3c, which points to the standard $Li_{1.3}Al_{0.3}Ti_{1.7}(PO_4)_3$ pattern (ICSD No. 427619). A small amount of $LiPO_3$ was identified. Nevertheless, the tiny amount of impurity could be formed by excess $LiCOOCH_3$ in the precursor which was used to compensate the Li loss at elevated calcination temperature.[12,50,51]

To investigate the ionic conductivity of LATP nanofibers, relatively dense pellets were prepared from the spun LATP fibers by a press-sintering method involving uniaxial die pressing, densification by isostatic cold pressing at 504 MPa for 30 seconds, and subsequent sintering at 900 °C for 4 hours. The thickness and surface roughness of the LATP pellets were controlled by polishing with P800 and P1200 sandpapers. The relative density of the produced ceramic substrates is about 89% of its theoretical density (2.93 g cm^{-3}). The electrolyte pellet was coated with ~300 nm Au layers on the surfaces and sandwiched between stainless steel blocking electrodes. The total Li^+ conductivity of LATP nanofiber electrolyte was characterized by electrochemical impedance spectroscopy (EIS). **Figure 2**d shows the typical Nyquist plots of the ceramic electrolyte in the combined high-frequency range of 3 GHz-10 MHz and normal-frequency range of 10 MHz-1 Hz at 25 °C. To allow a clear comparison between the grain conductivity and the grain boundary conductivity, the enlarged area in the high-frequency range, as represented in the insert image in **Figure 2**d, clearly shows the grain semicircle of the ceramic electrolyte. Therefore, the data are fitted using two RC series circuits, where the RC circuits at high and medium frequencies correspond to the responses of the grain and the grain boundary, respectively. According to Eq. 1 - 3 in the experimental section (Supplementary Information), the total, grain and grain boundary conductivities of the LATP

nanofiber electrolyte are 0.15 mS cm^{-1}, 3.1 mS cm^{-1} and 0.85×10^{-3} mS cm^{-1}, respectively, at 25 °C. While the slightly lower total ionic conductivity caused by the relatively low density of the pellets prepared by LATP fibers (relative density of 89% vs. above 92% in literature[12,51–53]), the value of the high grain conductivity of the LATP nanofiber electrolyte agrees well with previous reports,[12,52]. For LATP, the high resistances at the grain boundaries limit its total ionic conductivities,[53] the same is true for the LATP nanofibers. The reason for that has been attributed to the existence of less-conducting amorphous phases or disordered phases at grain boundary regions of LATP.[54] Hence, the specific grain boundary conductivity of the prepared ceramic electrolyte is about 4 orders of magnitude lower than its grain conductivity. Despite the low grain boundary conductivity, the total ionic conductivity of the prepared LATP nanofiber electrolyte at 25 °C is higher than most of the polymer electrolytes.[18,19]

Based on the conductivities at temperatures between -20 °C and 60 °C, grain, grain boundary and total activation energies (E_a) of the LATP nanofiber electrolyte are calculated based on Eq. 5 (Supporting Information). Arrhenius plots for fitting and calculating the E_a are shown in **Figure 2**e. The grain activation energy is 0.28 eV, whereas the grain boundary activation energy is 0.41 eV. The higher activation energy at the grain boundaries suggests that, as in most NASICON-type Li^+ conductors, the largest energy barrier to Li^+ motion within the polycrystalline structure is at the grain boundaries. The total activation energy is 0.37 eV, which is consistent with the previously reported value.[12] Overall, the highly conductive and well-interconnected LATP nanofibers provide fast continuous Li^+ transport channels in hybrid electrolyte. Besides, the tough nature of ceramic materials could guarantee the separation of the electrodes in all-solid-state Li batteries under severe conditions.[55]

2.3. Morphology and Electrochemical Performance of Hybrid Electrolyte.

Figure 3a shows the SEM and photographs of the free-standing hybrid electrolyte. As illustrated in the SEM image, no signs of pores between the intertwined LATP nanofibers

indicate the complete infiltration of polymer electrolyte into the ceramic fiber skeleton backbone. Moreover, although it is difficult to clearly determine the size of the ceramic fibers because they are embedded in the polymer, the overall length of the ceramic fibers appears to be shorter than that of the original LATP fibers, which could be due to the effect of the mixing process. While the incorporated 32 wt% of EC:DMC (1:1 vol/vol) plasticizers in the hybrid electrolyte, the membrane remains in the solid structure and exhibits good flexibility, as can be seen in the photographs in **Figure 3**a. The foldable hybrid electrolyte can then be used in the flexible Li-ion solid-state batteries.

The Li^+ transference number of the hybrid electrolyte was determined by a combination of chronoamperometry (CA) and EIS measurements. The detailed calculation is presented in the experimental section in the supplementary information. CA and EIS before and after the CA test at 25 °C are presented in **Figure 3**b. It can be observed that the current response to the applied static potential polarization first drops and then remains constant for the rest of the measurement. The resistance increased a little after the CA measurement. The Li^+ transference number of the hybrid electrolyte is calculated to be 0.94 which is slightly higher than the MEEP/LiSTFSI polymer (0.93, shown in Figure S5), close to unity, indicating a single-ion conducting behavior of both materials. The significantly high Li^+ transference number is mainly due to the restricted movement of anions as the part of crosslinking network in the MEEP/LiSTFSI polymer and the hybrid electrolyte.[43,56,57] Note the additional participation of the $STFSI^-$ anions in the photoinitiated radical-induced cross-linking via their terminal alkene groups which is a prerequisite for the immobilization of anions and the increased lithium ion transference number. Besides, the EC:DMC (1:1 vol/vol) plasticizers incorporated in the matrix of MEEP/LiSTFSI polymer and hybrid electrolyte contributed to the increase of Li^+ transference number. The predominant intentions of the plasticizers were a) to facilitate the dissociation of Li^+ cations, b) to increase the polymer segmental mobility, thus increasing

elasticity, c) to enhance the ability of flexible and continuous adhesion to the various interfaces (similar to the role of a binder stabilizing the interfaces and contacts of a microstructure) and, last not least, d) a facilitated impregnation of porous cathode composite structures (such as LFP used in this work).[58,59,60]

Temperature-dependent ionic conductivities of LATP nanofibers, MEEP/LiSTFSI polymer and hybrid electrolyte are presented in **Figure 3**c. At ambient temperatures (20-30 °C), the ionic conductivity of the hybrid electrolyte is in the range of 0.23 to 0.42 mS cm^{-1}, slightly lower than that of the MEEP/LiSTFSI polymer. This can be attributed to the considerably lower content of EC/DMC plasticizer in the hybrid electrolyte (32 wt% uptake) than in the pure polymer membrane (86 wt% uptake). The ionic conductivities of hybrid electrolyte at ambient temperatures are almost two times higher than that for 89% dense LATP nanofibers due to the high ionic conductivity of polymer electrolyte, the complete infiltration of polymer in the pores of LATP fibers, and the "active filler" effect of the ceramic in the hybrid electrolyte.[24] Such fillers not only possess the characteristics of inert ceramics that enhance the free volume of polymer and accelerate segmental dynamics but also provide additional ion-transport channels. Also, the LATP active fillers can increase the concentration of mobile Li^+, interfacial conduction, and anion attraction, thus improving ion transport of the hybrid electrolyte.[61] With further increasing temperature, the ionic conductivity of the hybrid electrolyte exceeded the values of MEEP/LiSTFSI polymer. At 60 °C, the ionic conductivity of hybrid electrolyte reached 1.9 mS cm^{-1}, which is comparable with the dense LATP electrolyte reported in literature at the same temperature.[12,15,50]

As illustrated in **Figure 3**d, the LSV measurements of MEEP/LiSTFSI polymer and hybrid electrolyte were performed at a voltage of 0 to 6 V at 25 °C. The onset decomposition potentials of MEEP/LiSTFSI polymer and hybrid electrolyte due to oxidation are up to 4.9 V and 5.4 V (vs. Li^+/Li), respectively. This suggests that both materials may be suitable for high-voltage Li

batteries. The high oxidation potential of MEEP/LiSTFSI polymer can be attributed to the suppressed migration of anions and thus limit or block their irreversible oxidation. The enhanced electrochemical window of hybrid electrolyte might be favored by the dipole-dipole interaction between polymer chains and LATP nanofibers which elevates the oxidation decomposition potential of the MEEP/LiSTFSI polymer.[61]

Li plating/stripping tests in Li symmetric cells were conducted to investigate the interfacial stability of the electrolyte and Li electrode. As demonstrated in **Figure 4**a, the high overpotential of the MEEP/LiSTFSI polymer is mainly attributed to the relatively large thickness of the membrane. Since the polymer is very soft, the polymer membrane was fabricated with a thickness of 500 μm to maintain the structural stability and the separation of the electrodes. The cell with the MEEP/LiSTFSI polymer showed stable cycling up to 1118 hours under a current density of 0.1 mA cm^{-2}. The good cycling stability of the polymer could be attributed to the fact that the anions are immobilized in the polymer - Li^+ can diffuse more easily from the bulk electrolyte onto the Li surface, providing a relatively stable and uniform interface for Li^+ deposition.[57] On the other hand, although it's known that LATP is unstable against metallic Li due to the rapid reduction of Ti^{4+},[15] the time-dependent voltage profile exhibits that the cell with the hybrid electrolyte is even more stable compared with the cell with the MEEP/LiSTFSI polymer under the same current density. The hybrid electrolyte is stable cycled up to 2000 hours with Li electrodes due to its advantages inherited from both MEEP/LiSTFSI polymer and LATP ceramic. The single-ion conducting polymer not only provides the continuous ion conducting pathway and isolates LATP from electrodes to avoid side reactions, but also offers soft contact with electrodes to reduce Li^+ transfer resistance cross the electrode-electrolyte interface. Meanwhile, the rigid LATP nanofibers offer expressways for the migration of Li^+ and enhance the mechanical strength of the electrolyte to suppress Li dendrites. These effects can be proved by comparing the surface morphologies of pristine Li

and Li electrodes being cycled with MEEP/LiSTFSI polymer and hybrid electrolyte, respectively, as the SEM images represented in **Figure 4**b. It is worth emphasizing that for the ambient sensitive Li anodes, an airtight K&W transfer module was used to transfer the samples from the glovebox directly to the SEM chamber. The module opens under vacuum in the SEM chamber hence avoids the exposure of the samples to the ambient atmosphere. As can be seen in the SEM images, after cycling in the cell with the polymer electrolyte, the mossy Li on the electrode surface is highly porous and rough. Besides, big cracks are formed due to long-term cycling. In contrast, the Li electrode cycled with hybrid electrolyte exhibits relatively smooth surface morphology except for the pits that formed typically during Li stripping.[62] These results indicate that the hybrid electrolyte is effective to regulate Li plating/stripping and thus restrain Li dendrite growth.

2.4. Battery Performance.

The obtained hybrid electrolytes were sandwiched between Li metal anode and $LiFePO_4$ cathode to assemble coin cells for battery tests. To ensure sufficient Li^+ conduction of the cathode, the $LiFePO_4$ cathode layer was coated with MEEP/LiSTFSI polymer and used as the substrate for fabricating the hybrid electrolyte.

Figure 5a shows the CV curves of Li|hybrid electrolyte|$LiFePO_4$ at different scan rates over the potential range of 2.2-4.2 V. Apart from the redox peaks of $LiFePO_4$, no additional oxidation or reduction peak of the cell is observed in the potential range. The potential intervals between redox peaks of $LiFePO_4$ are 0.52, 0.79 and 1.23 V at the scan rate of 0.1, 0.2 and 0.5 mV s^{-1}, respectively. When the scan rate increases, the potential interval becomes broader due to polarization. Moreover, the symmetrical redox peaks suggest good kinetics of the prepared cells even at the high scan rate of 0.5 mV s^{-1}. The prepared coin cells are able to light up LED at room temperature as shown in the photograph in **Figure 5**a. Hence, the cycling tests of the coin cells were performed initially at 25 °C.

As shown in the charge-discharge profiles obtained in the voltage range of 2.3-4.1 V in **Figure 5**b, apart from the low coulombic efficiency of the initial cycle at a low current rate of 0.05C, the coulombic efficiencies of the rest cycles are close to 100% despite the increased current rate. The specific discharge capacities of the cell are found to be 161, 160, 157, 132, 113 and 91 mAh g^{-1} at 0.05C, 0.1C, 0.2C, 0.5C, 1C, 1.5C, in their turns. With increasing the current rate, the discharge capacities faded and the overpotential increases, indicating the kinetic limitation of Li^+ transport in the electrolyte impedes the battery performance. The rate capacity at relevant current densities is represented in **Figure 5**c. As shown in the figure, stable discharge capacity can be delivered and high corresponding coulombic efficiency is achieved at all the current densities. Although the specific discharge capacity faded to about half of the theoretical capacity at 1.5C, the capacity can be recovered to the initial values when the C-rate turned back to 0.1C, indicating the good durability of the hybrid electrolyte at high overpotentials.

Li|hybrid electrolyte|$LiFePO_4$ cells were further cycled at elevated temperatures at a higher current rate of 1C, as the results are shown in **Figure 5**d. With increasing the temperature from 25 to 60 °C, the discharge capacity increased from ~68% to ~95% of its theoretical capacity, mainly owing to the promoted Li^+ transportation in the electrolyte, cathode and at the electrolyte/electrode interfaces. The maximum fluctuation of Coulombic efficiency is up to 3%, the average fluctuation being around 1%. The small fluctuation could be due to the overpotential caused by SEI growth at elevated temperatures.

Long-term cycling stability of the Li|hybrid electrolyte|$LiFePO_4$ battery is evaluated at a current rate of 0.5C at 25 °C. As shown in **Figure 6**a, the discharge capacity of the battery after 500 cycles is 122.7 mAh g^{-1}, corresponding to 93% retention of the initial capacity and 72.2% of the theoretical capacity of the $LiFePO_4$ cathode. Moreover, the coulombic efficiency of the battery is about 99% on average over all cycles. The good cycling performance of the battery

suggests that the established electrode/electrolyte interface can remain stable and compatible during the cycling.

According to the models proposed by Chazalviel[38,40,41] and Monroe[46], the ability to restrain Li dendrite growth is mainly due to the high Li^+ transference number, as well as the good mechanical strength of the hybrid electrolyte with the integrated ceramic nanowires.[49,63] As illustrated in **Figure 6**b, the conventional solid polymer electrolytes are merely a polymer matrix with a dissolved and dissociated Li-salt meaning independently mobile cations and anions, corresponding to "dual-ion based electrolytes". Applying an electric field will cause a migration of Li^+ and anions in opposite directions. In the steady-state, the net anion flux becomes zero, but at the cost of a salt concentration gradient which compensates any electric field-induced anion migration flux by an opposite anion diffusion flux in the concentration gradient leaving a mere lithium-ion flux. But the concentration gradient also leads to a lower steady-state lithium-ion current. This negative effect can only be considerably diminished by increasing the lithium-ion transference number to a value near 1. Hence, the disadvantage of independent mobility of cations and anions is compensated in the prepared hybrid electrolyte by immobilizing the anions. The resulting high transference number of lithium ions effectively prevents the formation of salt concentration gradients and concentrated lithium-ion flux, which suppresses the lithium dendrite growth.[43] In addition to the efficient suppression of Li dendrite growth, the hybrid electrolyte is capable to deal with varied interfacial stresses, assuring close contact with the electrodes since the LATP nanofiber skeleton is fully wet and coated with MEEP/LiSTFSI polymer. Moreover, the Li^+ migration ability in the hybrid electrolyte is boosted due to the synergistic transportations of single Li^+ conducting polymer and LATP. The LATP nanofibers can effectively increase the free volume of the polymer and enhance the mobility of chain segments close to the ceramic/polymer interface, beneficial for Li^+ transportation. On the other hand, the 3D interconnected LATP nanofibers offer long-range

fast Li^+ conductive pathways in the composite that can further promote Li^+ transfer efficiency. Overall, these results demonstrated promising applicability of the hybrid electrolyte to safer Li metal batteries for flexible electronic device applications.

3. CONCLUSION

In summary, single Li^+ conducting free-standing membranes of 3D interconnected NASICON-type ceramic-polymer composite were prepared for Li batteries. The LATP nanofiber networks were synthesized by electrospinning followed by high-temperature calcination, and were further used as the skeleton in hybrid electrolytes with a single Li^+ conducting polymer of MEEP/LiSTFSI. The hybrid electrolyte exhibited high ionic conductivity of 0.31 mS cm^{-1} at room temperature due to the synergistic effects of single Li^+ conducting polymer and 3D interconnected LATP nanofibers. Benefiting from the high Li^+ transference number (0.94), the hybrid electrolyte could effectively suppress Li dendrite growth that the symmetric Li|hybrid eletrolyte|Li cell runs for 2000 h at a current density of 0.1 mA cm^{-2} without any short circuit. Gain from these merits, the assembled Li|hybrid eletrolyte|$LiFePO_4$ cell demonstrated good rate capacity and stable long-term cycle performance. At 25 °C, it can keep a steady specific discharge capacity of ~113 mAh g^{-1} at 1C and maintain a discharge capacity of 122.7 mAh g^{-1} at 0.5C after 500 cycles, which is 93% retention of the initial capacity. The facile approach of single Li^+ conducting polymer-in-ceramic membrane provides one of the most promising electrolytes for safe, long-life, and high energy density Li metal batteries. Moreover, the 3D framework structure would also be applicable to other ceramic electrolyte systems, showing great promise in the applications in high-performance all-solid-state batteries.

ASSOCIATED CONTENT

Supporting Information The Supporting Information is available free of charge on the website or from the author.

Experimental section. Figure S1-S5. NMR measurements of LiSTFSI, ATR-IR spectrum of LiSTFSI and MEEP polymers. DC polarization

and Nyquist plots of the MEEP/LiSTFSI polymer before and after DC measurement. Table S1. The obtained data for the calculation of transference numbers.

AUTHOR INFORMATION

Corresponding Author

*E-mail: s.yu@fz-juelich.de

ORCID

Shicheng Yu 0000-0002-6619-3330

Qi Xu 0000-0001-5133-2281

Xin Lu 0000-0002-6631-7532

Zigeng Liu 0000-0002-2955-5080

Anna Windmüller 0000-0003-2829-3362

Chih-Long Tsai 0000-0001-8103-3514

Annika Buchheit 0000-0001-8131-3604

Hermann Tempel 0000-0002-9794-6403

Hans Kungl 0000-0003-3142-3906

Hans-D. Wiemhöfer 0000-0002-6049-9953

Rüdiger-A. Eichel 0000-0002-0013-6325

Author Contributions

The manuscript was written through contributions of all authors. All authors have given approval to the final version of the manuscript.

Notes

The authors declare no competing financial interest.

ACKNOWLEDGMENTS

This work was financially supported by the project of "Materials and Components to Meet High Energy Density Batteries III" of the funding program "Excellent battery" from the Bundesministerium für Bildung und Forschung (BMBF) (Project No.: 13XP0258B), and the project "High Performance Solid-State Batteries" (HIPSTER) from "Ministerium für Kultur und Wissenschaft des Landes Nordrhein-Westfalen".

REFERENCES

(1) Zheng, Y.; Yao, Y.; Ou, J.; Li, M.; Luo, D.; Dou, H.; Li, Z.; Amine, K.; Yu, A.; Chen, Z. A Review of Composite Solid-State Electrolytes for Lithium Batteries:

Fundamentals, Key Materials and Advanced Structures. *Chem. Soc. Rev.* **2020**, *49*, 8790–8839. https://doi.org/10.1039/d0cs00305k.

(2) Sheng, O.; Jin, C.; Ding, X.; Liu, T.; Wan, Y.; Liu, Y.; Nai, J.; Wang, Y.; Liu, C.; Tao, X. A Decade of Progress on Solid-State Electrolytes for Secondary Batteries: Advances and Contributions. *Adv. Funct. Mater.* **2021**, *31*, 2100891. https://doi.org/10.1002/adfm.202100891.

(3) Oh, P.; Lee, H.; Park, S.; Cha, H.; Kim, J.; Cho, J. Improvements to the Overpotential of All-Solid-State Lithium-Ion Batteries during the Past Ten Years. *Adv. Energy Mater.* **2020**, *10*, 2000904. https://doi.org/https://doi.org/10.1002/aenm.202000904.

(4) Ding, Z.; Li, J.; Li, J.; An, C. Review—Interfaces: Key Issue to Be Solved for All Solid-State Lithium Battery Technologies. *J. Electrochem. Soc.* **2020**, *167*, 070541. https://doi.org/10.1149/1945-7111/ab7f84.

(5) Boaretto, N.; Garbayo, I.; Valiyaveettil-SobhanRaj, S.; Quintela, A.; Li, C.; Casas-Cabanas, M.; Aguesse, F. Lithium Solid-State Batteries: State-of-the-Art and Challenges for Materials, Interfaces and Processing. *J. Power Sources* **2021**, *502*, 229919. https://doi.org/https://doi.org/10.1016/j.jpowsour.2021.229919.

(6) Zhang, X.; Wang, S.; Xue, C.; Xin, C.; Lin, Y.; Shen, Y.; Li, L.; Nan, C.-W. Self-Suppression of Lithium Dendrite in All-Solid-State Lithium Metal Batteries with Poly(Vinylidene Difluoride)-Based Solid Electrolytes. *Adv. Mater.* **2019**, *31*, 1806082. https://doi.org/https://doi.org/10.1002/adma.201806082.

(7) Zhou, D.; Shanmukaraj, D.; Tkacheva, A.; Armand, M.; Wang, G. Polymer Electrolytes for Lithium-Based Batteries: Advances and Prospects. *Chem* **2019**, *5*, 2326–2352. https://doi.org/10.1016/j.chempr.2019.05.009.

(8) Baskoro, F.; Wong, H. Q.; Yen, H.-J. Strategic Structural Design of a Gel Polymer Electrolyte toward a High Efficiency Lithium-Ion Battery. *ACS Appl. Energy Mater.* **2019**, *2*, 3937–3971. https://doi.org/10.1021/acsaem.9b00295.

(9) Lopez, J.; Mackanic, D. G.; Cui, Y.; Bao, Z. Designing Polymers for Advanced Battery Chemistries. *Nat. Rev. Mater.* **2019**, *4*, 312–330. https://doi.org/10.1038/s41578-019-0103-6.

(10) Famprikis, T.; Canepa, P.; Dawson, J. A.; Islam, M. S.; Masquelier, C. Fundamentals of Inorganic Solid-State Electrolytes for Batteries. *Nat. Mater.* **2019**, *18*, 1278–1291. https://doi.org/10.1038/s41563-019-0431-3.

(11) Wang, C.; Fu, K.; Kammampata, S. P.; McOwen, D. W.; Samson, A. J.; Zhang, L.; Hitz, G. T.; Nolan, A. M.; Wachsman, E. D.; Mo, Y.; Thangadurai, V.; Hu, L. Garnet-Type Solid-State Electrolytes: Materials, Interfaces, and Batteries. *Chem. Rev.* **2020**, *120*, 4257–4300. https://doi.org/10.1021/acs.chemrev.9b00427.

(12) Xu, Q.; Tsai, C.-L.; Song, D.; Basak, S.; Kungl, H.; Tempel, H.; Hausen, F.; Yu, S.; Eichel, R.-A. Insights into the Reactive Sintering and Separated Specific Grain/Grain Boundary Conductivities of $Li_{1.3}Al_{0.3}Ti_{1.7}(PO_4)_3$. *J. Power Sources* **2021**, *492*, 229631. https://doi.org/https://doi.org/10.1016/j.jpowsour.2021.229631.

(13) Tsai, C.-L.; Yu, S.; Tempel, H.; Kungl, H.; Eichel, R.-A. All-Ceramic Li Batteries Based on Garnet Structured $Li_7La_3Zr_2O_{12}$. *Mater. Technol.* **2020**, *35*, 656–674. https://doi.org/10.1080/10667857.2020.1746539.

(14) Yu, X.; Manthiram, A. A Review of Composite Polymer-Ceramic Electrolytes for Lithium Batteries. *Energy Storage Mater.* **2021**, *34*, 282–300. https://doi.org/https://doi.org/10.1016/j.ensm.2020.10.006.

(15) Yu, S.; Schmohl, S.; Liu, Z.; Hoffmeyer, M.; Schön, N.; Hausen, F.; Tempel, H.; Kungl, H.; Wiemhöfer, H. D.; Eichel, R. A. Insights into a Layered Hybrid Solid Electrolyte and Its Application in Long Lifespan High-Voltage All-Solid-State Lithium Batteries. *J. Mater. Chem. A* **2019**, *7*, 3882–3894. https://doi.org/10.1039/c8ta11259b.

(16) Sun, C.; Liu, J.; Gong, Y.; Wilkinson, D. P.; Zhang, J. Recent Advances in All-Solid-State Rechargeable Lithium Batteries. *Nano Energy*. 2017, *33*, 363–386. https://doi.org/10.1016/j.nanoen.2017.01.028.

(17) Zhang, B.; Tan, R.; Yang, L.; Zheng, J.; Zhang, K.; Mo, S.; Lin, Z.; Pan, F. Mechanisms and Properties of Ion-Transport in Inorganic Solid Electrolytes. *Energy Storage Mater.* **2018**, *10*, 139–159. https://doi.org/https://doi.org/10.1016/j.ensm.2017.08.015.

(18) Quartarone, E.; Mustarelli, P. Electrolytes for Solid-State Lithium Rechargeable Batteries: Recent Advances and Perspectives. *Chem. Soc. Rev.* **2011**, *40*, 2525–2540. https://doi.org/10.1039/C0CS00081G.

(19) Xue, Z.; He, D.; Xie, X. Poly(Ethylene Oxide)-Based Electrolytes for Lithium-Ion Batteries. *J. Mater. Chem. A* **2015**, *3*, 19218–19253. https://doi.org/10.1039/C5TA03471J.

(20) Long, L.; Wang, S.; Xiao, M.; Meng, Y. Polymer Electrolytes for Lithium Polymer Batteries. *J. Mater. Chem. A* **2016**, *4*, 10038–10069. https://doi.org/10.1039/C6TA02621D.

(21) Lin, D.; Liu, W.; Liu, Y.; Lee, H. R.; Hsu, P.-C.; Liu, K.; Cui, Y. High Ionic Conductivity of Composite Solid Polymer Electrolyte via In Situ Synthesis of Monodispersed SiO_2 Nanospheres in Poly(Ethylene Oxide). *Nano Lett.* **2016**, *16*, 459–465. https://doi.org/10.1021/acs.nanolett.5b04117.

(22) Pan, Q.; Smith, D. M.; Qi, H.; Wang, S.; Li, C. Y. Hybrid Electrolytes with Controlled Network Structures for Lithium Metal Batteries. *Adv. Mater.* **2015**, *27*, 5995–6001. https://doi.org/https://doi.org/10.1002/adma.201502059.

(23) Croce, F.; Persi, L. L.; Scrosati, B.; Serraino-Fiory, F.; Plichta, E.; Hendrickson, M. A. Role of the Ceramic Fillers in Enhancing the Transport Properties of Composite Polymer Electrolytes. *Electrochim. Acta* **2001**, *46*, 2457–2461. https://doi.org/10.1016/S0013-4686(01)00458-3.

(24) Zhang, D.; Xu, X.; Qin, Y.; Ji, S.; Huo, Y.; Wang, Z.; Liu, Z.; Shen, J.; Liu, J. Recent Progress in Organic–Inorganic Composite Solid Electrolytes for All-Solid-State Lithium Batteries. *Chem. - A Eur. J.* **2020**, *26*, 1720–1736. https://doi.org/10.1002/chem.201904461.

(25) Lin, Y.; Wang, X.; Liu, J.; Miller, J. D. Natural Halloysite Nano-Clay Electrolyte for Advanced All-Solid-State Lithium-Sulfur Batteries. *Nano Energy* **2017**, *31*, 478–485. https://doi.org/https://doi.org/10.1016/j.nanoen.2016.11.045.

(26) Liu, W.; Liu, N.; Sun, J.; Hsu, P.-C.; Li, Y.; Lee, H.-W.; Cui, Y. Ionic Conductivity Enhancement of Polymer Electrolytes with Ceramic Nanowire Fillers. *Nano Lett.* **2015**, *15*, 2740–2745. https://doi.org/10.1021/acs.nanolett.5b00600.

(27) Chen, X.; Vereecken, P. M. Solid and Solid-Like Composite Electrolyte for Lithium Ion Batteries: Engineering the Ion Conductivity at Interfaces. *Adv. Mater. Interfaces* **2019**, *6*, 1800899. https://doi.org/https://doi.org/10.1002/admi.201800899.

(28) Shim, J.; Kim, H. J.; Kim, B. G.; Kim, Y. S.; Kim, D.-G.; Lee, J.-C. 2D Boron Nitride Nanoflakes as a Multifunctional Additive in Gel Polymer Electrolytes for Safe, Long Cycle Life and High Rate Lithium Metal Batteries. *Energy Environ. Sci.* **2017**, *10*, 1911–

1916. https://doi.org/10.1039/C7EE01095H.

(29) Yang, T.; Zheng, J.; Cheng, Q.; Hu, Y.-Y.; Chan, C. K. Composite Polymer Electrolytes with $Li_7La_3Zr_2O_{12}$ Garnet-Type Nanowires as Ceramic Fillers: Mechanism of Conductivity Enhancement and Role of Doping and Morphology. *ACS Appl. Mater. Interfaces* **2017**, *9*, 21773–21780. https://doi.org/10.1021/acsami.7b03806.

(30) Liu, W.; Lee, S. W.; Lin, D.; Shi, F.; Wang, S.; Sendek, A. D.; Cui, Y. Enhancing Ionic Conductivity in Composite Polymer Electrolytes with Well-Aligned Ceramic Nanowires. *Nat. Energy* **2017**, *2*, 17035. https://doi.org/10.1038/nenergy.2017.35.

(31) Zhai, H.; Xu, P.; Ning, M.; Cheng, Q.; Mandal, J.; Yang, Y. A Flexible Solid Composite Electrolyte with Vertically Aligned and Connected Ion-Conducting Nanoparticles for Lithium Batteries. *Nano Lett.* **2017**, *17*, 3182–3187. https://doi.org/10.1021/acs.nanolett.7b00715.

(32) Li, Z.; Huang, H.-M.; Zhu, J.-K.; Wu, J.-F.; Yang, H.; Wei, L.; Guo, X. Ionic Conduction in Composite Polymer Electrolytes: Case of PEO:Ga-LLZO Composites. *ACS Appl. Mater. Interfaces* **2019**, *11*, 784–791. https://doi.org/10.1021/acsami.8b17279.

(33) Wirtz, M.; Linhorst, M.; Veelken, P.; Tempel, H.; Kungl, H.; Moerschbacher, B. M.; Eichel, R.-A. Polyethylene Oxide-$Li_{6.5}La_3Zr_{1.5}Ta_{0.5}O_{12}$ Hybrid Electrolytes: Lithium Salt Concentration and Biopolymer Blending. *Electrochem. Sci. Adv.* **2021**, *1*, e2000029. https://doi.org/https://doi.org/10.1002/elsa.202000029.

(34) Zheng, J.; Tang, M.; Hu, Y.-Y. Lithium Ion Pathway within $Li_7La_3Zr_2O_{12}$-Polyethylene Oxide Composite Electrolytes. *Angew. Chemie Int. Ed.* **2016**, *55*, 12538–12542.

https://doi.org/https://doi.org/10.1002/anie.201607539.

(35) Wang, W.; Yi, E.; Fici, A. J.; Laine, R. M.; Kieffer, J. Lithium Ion Conducting Poly(Ethylene Oxide)-Based Solid Electrolytes Containing Active or Passive Ceramic Nanoparticles. *J. Phys. Chem. C* **2017**, *121*, 2563–2573. https://doi.org/10.1021/acs.jpcc.6b11136.

(36) Zheng, J.; Hu, Y.-Y. New Insights into the Compositional Dependence of Li-Ion Transport in Polymer–Ceramic Composite Electrolytes. *ACS Appl. Mater. Interfaces* **2018**, *10*, 4113–4120. https://doi.org/10.1021/acsami.7b17301.

(37) Liu, H.; Cheng, X.-B.; Huang, J.-Q.; Yuan, H.; Lu, Y.; Yan, C.; Zhu, G.-L.; Xu, R.; Zhao, C.-Z.; Hou, L.-P.; He, C.; Kaskel, S.; Zhang, Q. Controlling Dendrite Growth in Solid-State Electrolytes. *ACS Energy Lett.* **2020**, *5*, 833–843. https://doi.org/10.1021/acsenergylett.9b02660.

(38) Brissot, C.; Rosso, M.; Chazalviel, J.-N.; Lascaud, S. Dendritic Growth Mechanisms in Lithium/Polymer Cells. *J. Power Sources* **1999**, *81–82*, 925–929. https://doi.org/https://doi.org/10.1016/S0378-7753(98)00242-0.

(39) Golozar, M.; Hovington, P.; Paolella, A.; Bessette, S.; Lagacé, M.; Bouchard, P.; Demers, H.; Gauvin, R.; Zaghib, K. In Situ Scanning Electron Microscopy Detection of Carbide Nature of Dendrites in Li–Polymer Batteries. *Nano Lett.* **2018**, *18*, 7583–7589. https://doi.org/10.1021/acs.nanolett.8b03148.

(40) Brissot, C.; Rosso, M.; Chazalviel, J. -N.; Lascaud, S. In Situ Concentration Cartography in the Neighborhood of Dendrites Growing in Lithium/Polymer-Electrolyte/Lithium Cells. *J. Electrochem. Soc.* **1999**, *146*, 4393–4400. https://doi.org/10.1149/1.1392649.

(41) Chazalviel, J.-N. Electrochemical Aspects of the Generation of Ramified Metallic Electrodeposits. *Phys. Rev. A* **1990**, *42*, 7355–7367. https://doi.org/10.1103/PhysRevA.42.7355.

(42) Xu, W.; Wang, J.; Ding, F.; Chen, X.; Nasybulin, E.; Zhang, Y.; Zhang, J.-G. Lithium Metal Anodes for Rechargeable Batteries. *Energy Environ. Sci.* **2014**, *7*, 513–537. https://doi.org/10.1039/C3EE40795K.

(43) Deng, K.; Qin, J.; Wang, S.; Ren, S.; Han, D.; Xiao, M.; Meng, Y. Effective Suppression of Lithium Dendrite Growth Using a Flexible Single-Ion Conducting Polymer Electrolyte. *Small* **2018**, *14*, 1801420. https://doi.org/https://doi.org/10.1002/smll.201801420.

(44) Meziane, R.; Bonnet, J. P.; Courty, M.; Djellab, K.; Armand, M. Single-Ion Polymer Electrolytes Based on a Delocalized Polyanion for Lithium Batteries. *Electrochim. Acta* **2011**, *57*, 14–19. https://doi.org/10.1016/j.electacta.2011.03.074.

(45) Bouchet, R.; Maria, S.; Meziane, R.; Aboulaich, A.; Lienafa, L.; Bonnet, J.-P.; Phan, T. N. T.; Bertin, D.; Gigmes, D.; Devaux, D.; Denoyel, R.; Armand, M. Single-Ion BAB Triblock Copolymers as Highly Efficient Electrolytes for Lithium-Metal Batteries. *Nat. Mater.* **2013**, *12*, 452–457. https://doi.org/10.1038/nmat3602.

(46) Monroe, C.; Newman, J. The Impact of Elastic Deformation on Deposition Kinetics at Lithium/Polymer Interfaces. *J. Electrochem. Soc.* **2005**, *152*, A396–A404. https://doi.org/10.1149/1.1850854.

(47) Yin, X.; Wang, L.; Kim, Y.; Ding, N.; Kong, J.; Safanama, D.; Zheng, Y.; Xu, J.; Repaka, D. V. M.; Hippalgaonkar, K.; Lee, S. W.; Adams, S.; Zheng, G. W. Thermal Conductive 2D Boron Nitride for High-Performance All-Solid-State Lithium–Sulfur

Batteries. *Adv. Sci.* **2020**, *7*, 2001303. https://doi.org/https://doi.org/10.1002/advs.202001303.

(48) Zhang, D.; Xu, X.; Ji, S.; Wang, Z.; Liu, Z.; Shen, J.; Hu, R.; Liu, J.; Zhu, M. Solvent-Free Method Prepared a Sandwich-like Nanofibrous Membrane-Reinforced Polymer Electrolyte for High-Performance All-Solid-State Lithium Batteries. *ACS Appl. Mater. Interfaces* **2020**, *12*, 21586–21595. https://doi.org/10.1021/acsami.0c02291.

(49) Sheng, O.; Jin, C.; Luo, J.; Yuan, H.; Huang, H.; Gan, Y.; Zhang, J.; Xia, Y.; Liang, C.; Zhang, W.; Tao, X. $Mg_2B_2O_5$ Nanowire Enabled Multifunctional Solid-State Electrolytes with High Ionic Conductivity, Excellent Mechanical Properties, and Flame-Retardant Performance. *Nano Lett.* **2018**, *18*, 3104–3112. https://doi.org/10.1021/acs.nanolett.8b00659.

(50) Yu, S.; Mertens, A.; Gao, X.; Gunduz, D. C.; Schierholz, R.; Benning, S.; Hausen, F.; Mertens, J.; Kungl, H.; Tempel, H.; Eichel, R.-A. Influence of Microstructure and $AlPO_4$ Secondary-Phase on the Ionic Conductivity of $Li_{1.3}Al_{0.3}Ti_{1.7}(PO_4)_3$ Solid-State Electrolyte. *Funct. Mater. Lett.* **2016**, *9*, 1650066. https://doi.org/10.1142/S1793604716500661.

(51) Yu, S.; Mertens, A.; Tempel, H.; Schierholz, R.; Kungl, H.; Eichel, R.-A. Monolithic All-Phosphate Solid-State Lithium-Ion Battery with Improved Interfacial Compatibility. *ACS Appl. Mater. Interfaces* **2018**, *10*, 22264–22277. https://doi.org/10.1021/acsami.8b05902.

(52) Rettenwander, D.; Welzl, A.; Pristat, S.; Tietz, F.; Taibl, S.; Redhammer, G. J.; Fleig, J. A Microcontact Impedance Study on NASICON-Type $Li_{1+x}Al_xTi_{2-x}(PO_4)_3$ ($0 \leq x \leq 0.5$) Single Crystals. *J. Mater. Chem. A* **2016**, *4*, 1506–1513.

https://doi.org/10.1039/C5TA08545D.

(53) DeWees, R.; Wang, H. Synthesis and Properties of NaSICON-Type LATP and LAGP Solid Electrolytes. *ChemSusChem* **2019**, *12*, 3713–3725. https://doi.org/https://doi.org/10.1002/cssc.201900725.

(54) Kwatek, K.; Ślubowska, W.; Trébosc, J.; Lafon, O.; Nowiński, J. L. Structural and Electrical Properties of Ceramic Li-Ion Conductors Based on $Li_{1.3}Al_{0.3}Ti_{1.7}(PO_4)_3$-LiF. *J. Eur. Ceram. Soc.* **2020**, *40*, 85–93. https://doi.org/https://doi.org/10.1016/j.jeurceramsoc.2019.08.032.

(55) Kotobuki, M. Recent Progress of Ceramic Electrolytes for Post Li and Na Batteries. *Funct. Mater. Lett.* **2021**, *14*, 2130003. https://doi.org/10.1142/S1793604721300036.

(56) Zhang, D.; Xu, X.; Huang, X.; Shi, Z.; Wang, Z.; Liu, Z.; Hu, R.; Liu, J.; Zhu, M. A Flexible Composite Solid Electrolyte with a Highly Stable Interphase for Dendrite-Free and Durable All-Solid-State Lithium Metal Batteries. *J. Mater. Chem. A* **2020**, *8*, 18043–18054. https://doi.org/10.1039/d0ta06697d.

(57) Zhang, J.; Wang, S.; Han, D.; Xiao, M.; Sun, L.; Meng, Y. Lithium (4-Styrenesulfonyl) (Trifluoromethanesulfonyl) Imide Based Single-Ion Polymer Electrolyte with Superior Battery Performance. *Energy Storage Mater.* **2020**, *24*, 579–587. https://doi.org/https://doi.org/10.1016/j.ensm.2019.06.029.

(58) Bishop, A. G.; MacFarlane, D. R.; McNaughton, D.; Forsyth, M. Triflate Ion Association in Plasticized Polymer Electrolytes. *Solid State Ionics* **1996**, *85*, 129–135. https://doi.org/10.1016/0167-2738(96)00049-5.

(59) Park, U. S.; Hong, Y. J.; Oh, S. M. Fluorescence Spectroscopy for Local Viscosity

Measurements in Polyacrylonitrile (PAN)-Based Polymer Gel Electrolytes. *Electrochim. Acta* **1996**, *41*, 849–855. https://doi.org/10.1016/0013-4686(95)00372-X.

(60) Chandrasekaran, R.; Selladurai, S. Preparation and Characterization of a New Polymer Electrolyte (PEO:$NaClO_3$) for Battery Application. *J. Solid State Electrochem.* **2001**, *5*, 355–361. https://doi.org/10.1007/s100080000156.

(61) Li, S.; Zhang, S.-Q.; Shen, L.; Liu, Q.; Ma, J.-B.; Lv, W.; He, Y.-B.; Yang, Q.-H. Progress and Perspective of Ceramic/Polymer Composite Solid Electrolytes for Lithium Batteries. *Adv. Sci.* **2020**, *7*, 1903088. https://doi.org/https://doi.org/10.1002/advs.201903088.

(62) Liu, H.; Cheng, X.-B.; Xu, R.; Zhang, X.-Q.; Yan, C.; Huang, J.-Q.; Zhang, Q. Plating/Stripping Behavior of Actual Lithium Metal Anode. *Adv. Energy Mater.* **2019**, *9*, 1902254. https://doi.org/https://doi.org/10.1002/aenm.201902254.

(63) Sheng, O.; Zheng, J.; Ju, Z.; Jin, C.; Wang, Y.; Chen, M.; Nai, J.; Liu, T.; Zhang, W.; Liu, Y.; Tao, X. In Situ Construction of a LiF-Enriched Interface for Stable All-Solid-State Batteries and Its Origin Revealed by Cryo-TEM. *Adv. Mater.* **2020**, *32*, 2000223. https://doi.org/10.1002/adma.202000223.

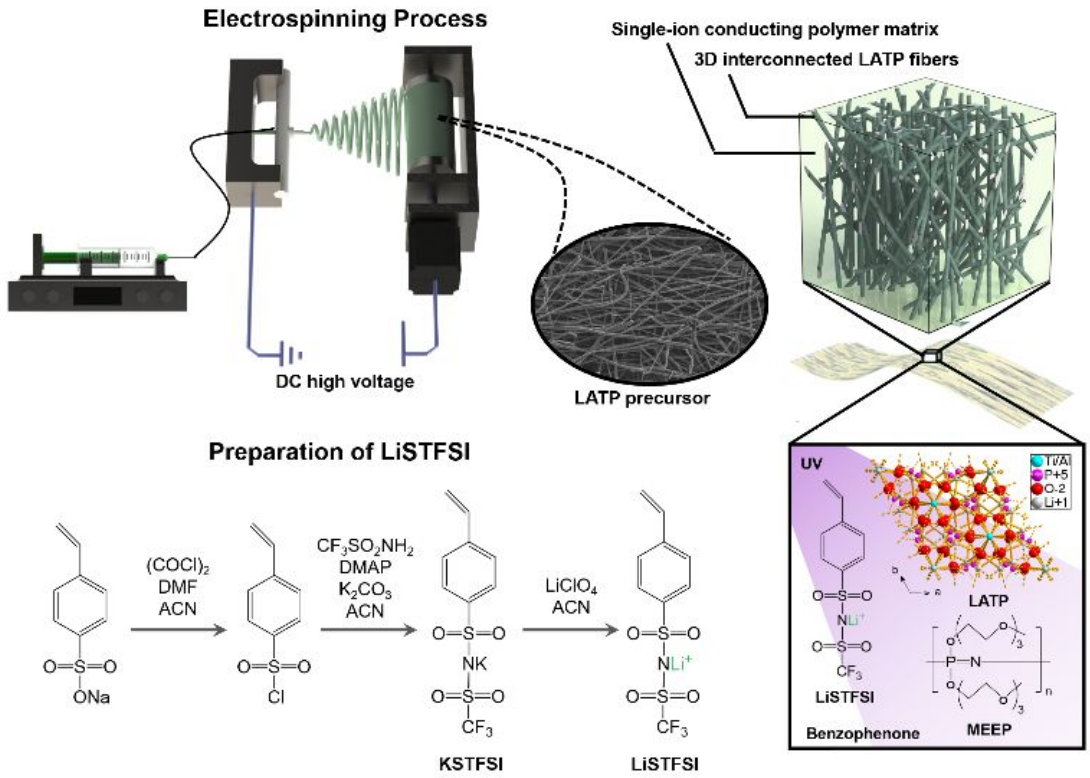

Figure 1 Schematic drawing of the electrospinning process of LATP nanofibers, preparation of LiSTFSI and hybrid electrolyte.

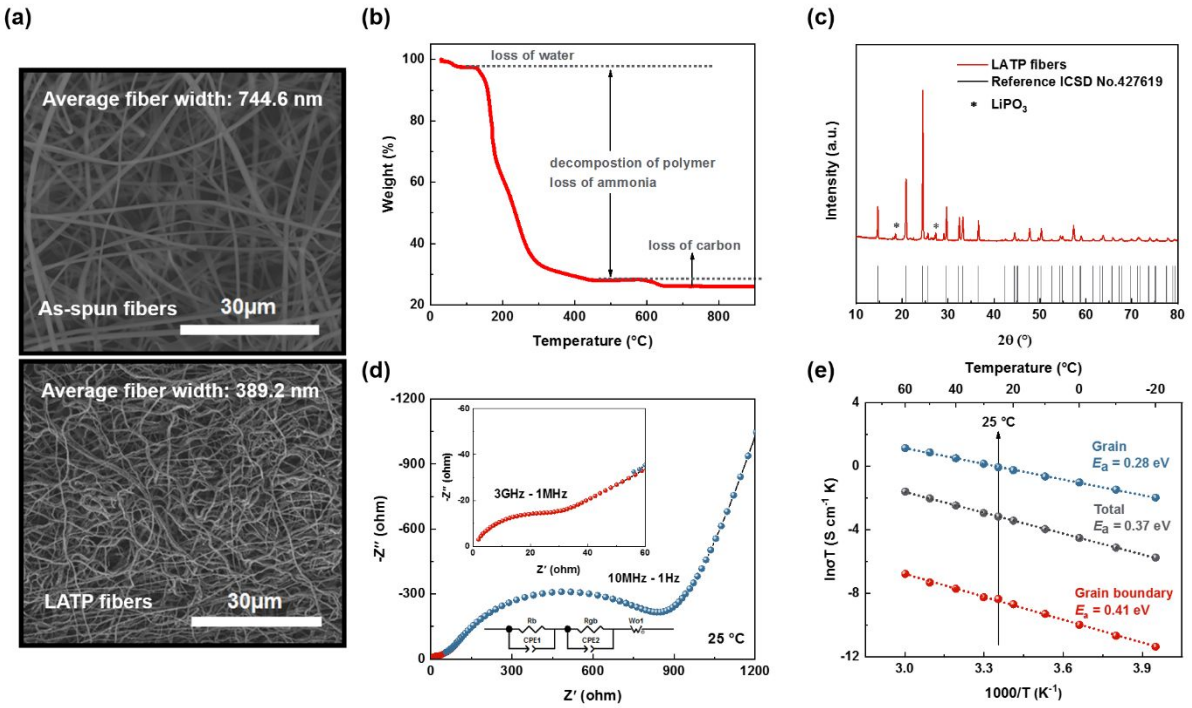

Figure 2 (a) SEM of as-spun and calcined LATP nanofibers. (b) TGA of as-spun LATP nanofibers. (c) XRD of LATP nanofibers after calcination at 900 °C in air. (d) Nyquist plot at 25 °C and (e) Arrhenius plot of LATP nanofiber electrolyte.

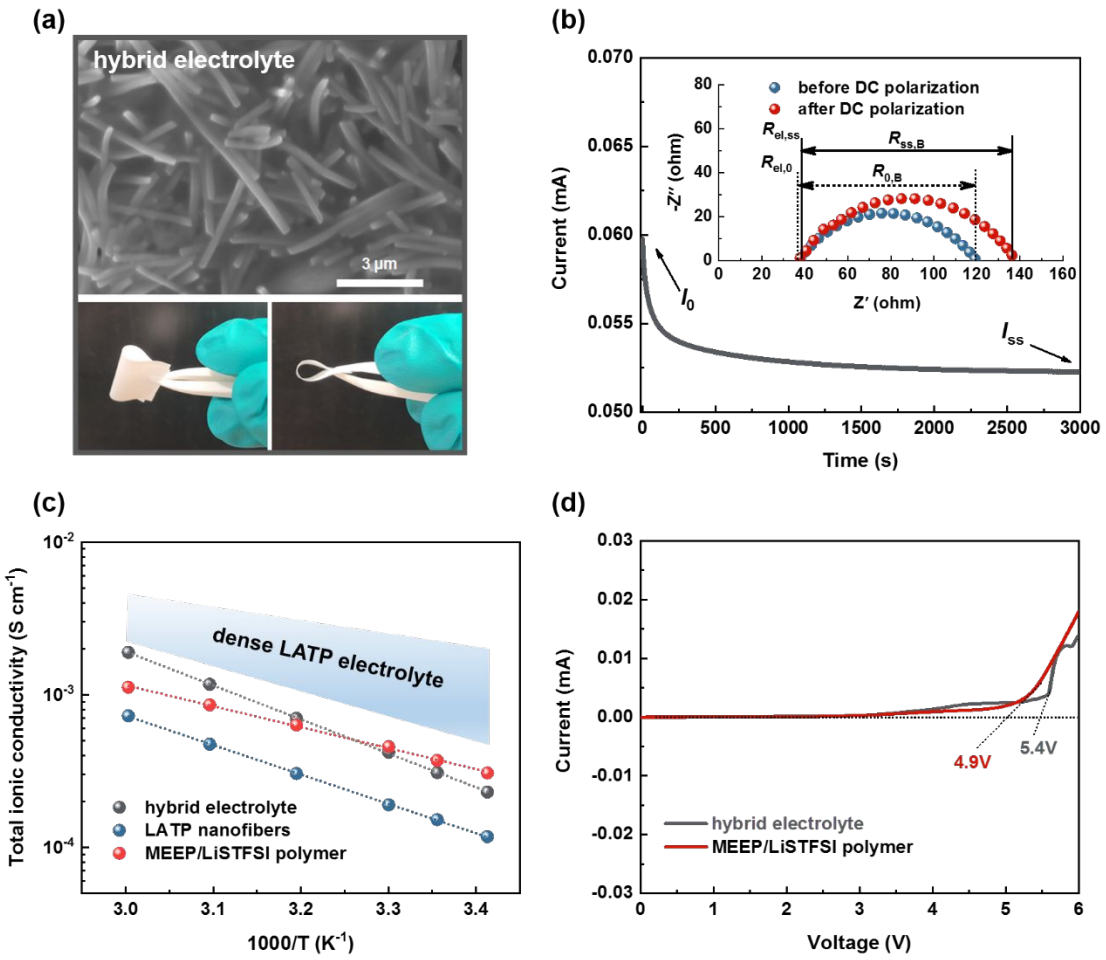

Figure 3 (a) SEM and photographs of free-standing hybrid electrolyte. (b) The evolution of current with polarization time under a polarization voltage of 0.01 V and Nyquist plots of the impedance of hybrid electrolyte before and after DC polarization at 25 °C. (c) Temperature dependent ionic conductivity of LATP nanofibers, MEEP/LiSTFSI polymer and hybrid electrolyte. The ionic conductivities of dense LATP were recalculated from Ref.[12,15,50]. (d) Linear sweep voltammetry for MEEP/LiSTFSI polymer and hybrid electrolyte in Li|electrolyte|SS cells, respectively, with a scan rate of 1 mV s^{-1} at 25 °C.

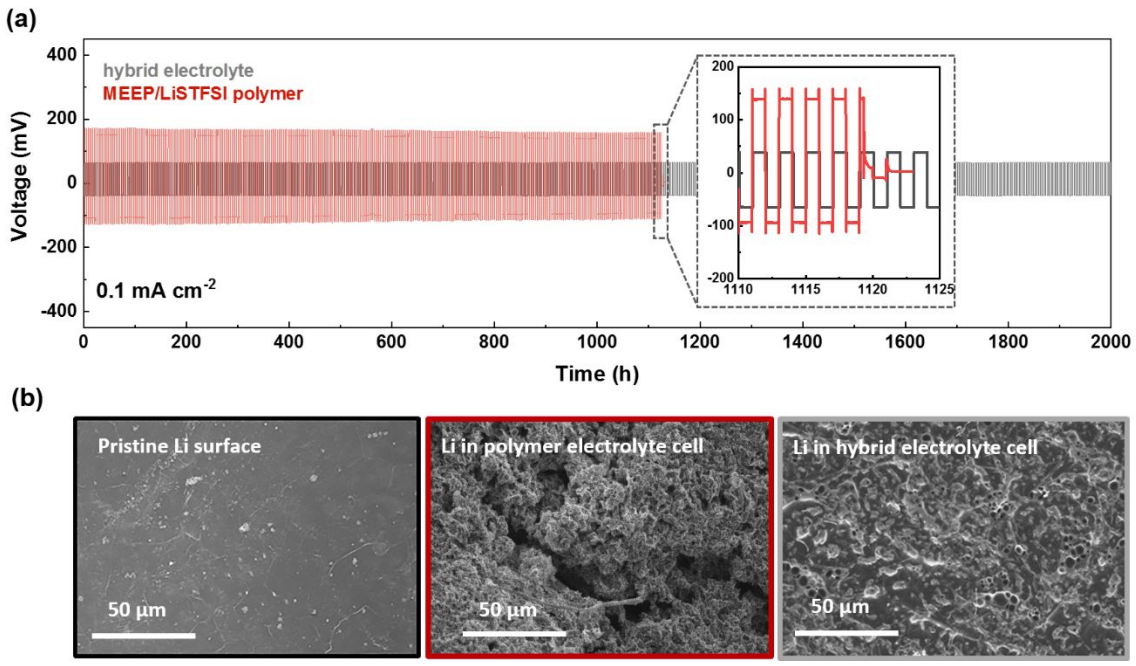

Figure 4 (a) Li plating/stripping test of MEEP/LiSTFSI polymer and hybrid electrolyte in Li symmetric cells, respectively, under a current density of 0.1 mA cm^{-2} at 25 °C. (b) SEM images of pristine Li anode (black border), Li anode cycled in contact with MEEP/LiSTFSI polymer (red border), and Li anode cycled in contact with hybrid electrolyte (grey border). A K&W transfer module was used to transfer the Li samples from the glovebox directly to the SEM chamber without exposing to ambient atmosphere.

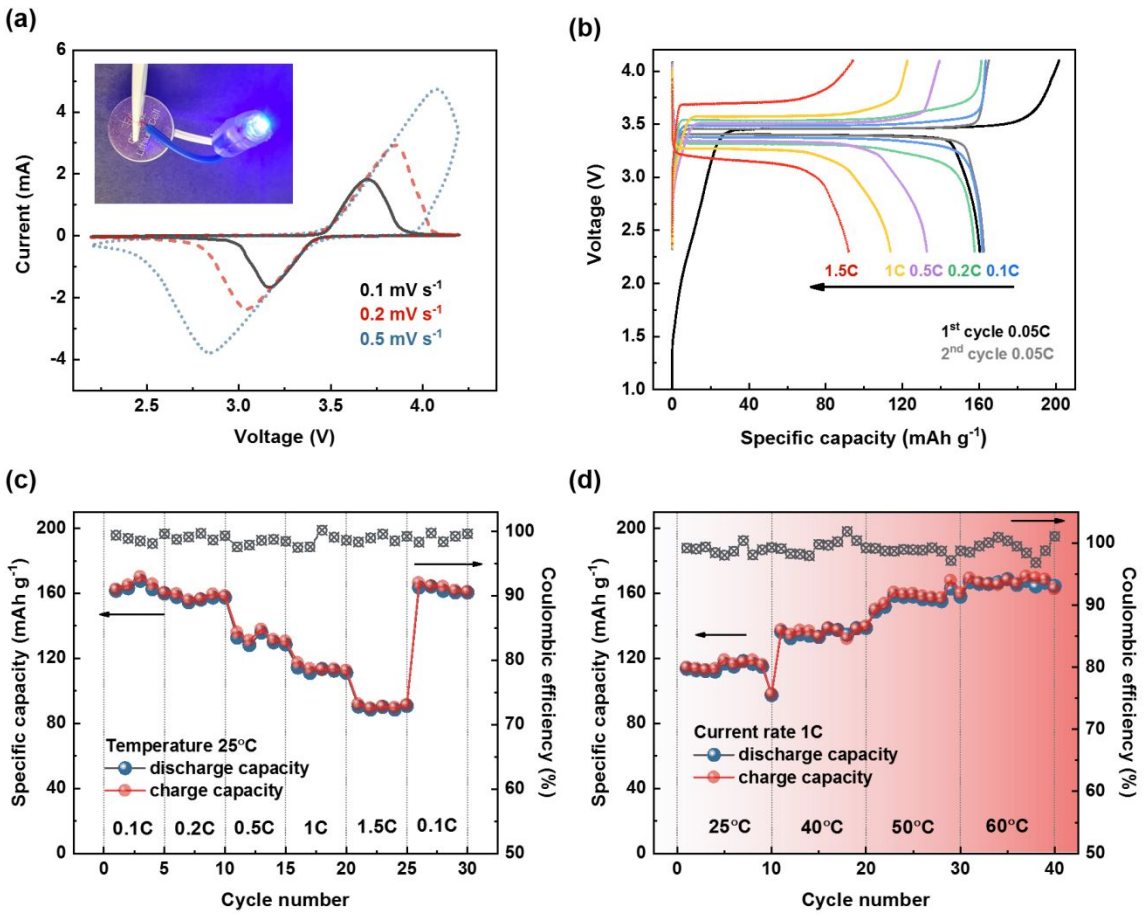

Figure 5 (a) CV curves of Li|hybrid electrolyte|$LiFePO_4$ cell measured in the voltage range of 2.2 to 4.2 V at different scanning rate of 0.1, 0.2 and 0.5 mV s^{-1}, respectively. The insert in (a) is LED lit up by the prepared battery. (b) Charge-discharge profiles in the voltage range of 2.3 to 4.1 V at C-rates of 0.05, 0.1, 0.2, 0.5, 1 and 1.5, respectively. (c) Rate performance of the Li|hybrid electrolyte|$LiFePO_4$ cell. And (d) temperature-dependent cycling performance of Li|hybrid electrolyte|$LiFePO_4$ coin cells at 1C at 25, 40, 50 and 60 °C, respectively. The measurements in (a-c) were carried out at 25 °C.

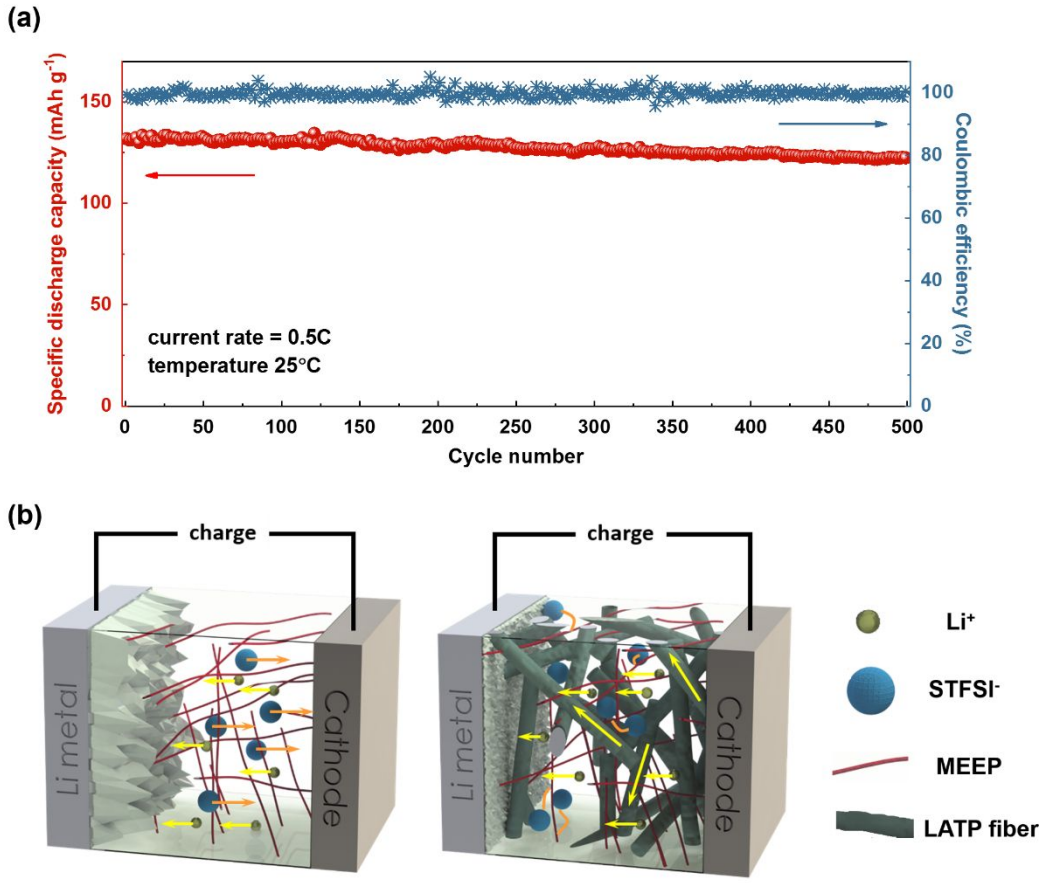

Figure 6 (a) Cycling performance of Li|hybrid electrolyte|$LiFePO_4$ cell with current rate of 0.5C at 25 °C. (b) Schematic illustration of Li dendrite growth in conventional "dual-ion conducting" polymer electrolytes (left) and Li dendrite suppression effect of the "single-ion conducting" hybrid electrolyte.

TABLE OF CONTENTS